doi:10.1093/brain/awz270 BRAIN 2019: 142; 3428–3439 | 3428

BRAIN
A JOURNAL OF NEUROLOGY

Dynamic modular-level alterations of structural-functional coupling in clinically isolated syndrome

Ismail Koubiyr,[1,2] Pierre Besson,[3,4] Mathilde Deloire,[5] Julie Charre-Morin,[5] Aurore Saubusse,[5] Thomas Tourdias,[1,2,5] Bruno Brochet[1,2,5] and Aurélie Ruet[1,2,5]

Structural and functional connectivity abnormalities have been reported previously in multiple sclerosis. However, little is known about how each modality evolution relates to the other. Recent studies in other neurological disorders have suggested that structural-functional coupling may be more sensitive in detecting brain alterations than any single modality. Accordingly, this study aimed to investigate the longitudinal evolution of structural-functional coupling, both at the global and modular levels, in the first year following clinically isolated syndrome. We hypothesized that during the course of multiple sclerosis, patients exhibit a decoupling between functional and structural connectivity due to the disruptive nature of the disease. Forty-one consecutive patients with clinically isolated syndrome were prospectively enrolled in this study, along with 19 age-, sex- and educational level-matched healthy control subjects. These participants were followed for 1 year and underwent resting-state functional MRI and diffusion tensor imaging at each time point, along with an extensive neuropsychological assessment. Graph theory analysis revealed structural reorganization at baseline that appeared as an increase in the clustering coefficient in patients compared to controls ($P < 0.05$), as well as modular-specific alterations. After 1 year of follow-up, both structural and functional reorganization was depicted with abnormal modular-specific connectivity and an increase of the functional betweenness centrality in patients compared to controls ($P < 0.01$). More importantly, structural-functional decoupling was observed in the salience, visual and somatomotor networks. These alterations were present along with preserved cognitive performance at this stage. These results depict structural damage preceding functional reorganization at a global and modular level during the first year following clinically isolated syndrome along with normal cognitive performance, suggesting a compensation mechanism at this stage of the disease. Principally, structural-functional decoupling observed for the first time in multiple sclerosis suggests that functional reorganization occurs along indirect anatomical pathways.

1 University of Bordeaux, F-33000 Bordeaux, France
2 Inserm U1215 - Neurocentre Magendie, F-33000 Bordeaux, France
3 Department of Radiology, Northwestern University, Feinberg School of Medicine, Chicago, IL, USA
4 Department of Neurological Surgery, Northwestern University, Feinberg School of Medicine, Chicago, IL, USA
5 CHU de Bordeaux, F-33000 Bordeaux, France

Correspondence to: Prof. Bruno Brochet
CHU Pellegrin,
Place Amélie Raba Léon
33000 Bordeaux, France
E-mail: bruno.brochet@chu-bordeaux.fr

Keywords: multiple sclerosis; clinically isolated syndrome; functional MRI; diffusion tensor imaging; graph theory

Abbreviations: CIS = clinically isolated syndrome; MSFC = Multiple Sclerosis Functional Composite

Received March 19, 2019. Revised June 24, 2019. Accepted July 11, 2019. Advance Access publication September 5, 2019

Introduction

Clinically isolated syndrome (CIS) is a single neurological episode that may be suggestive of multiple sclerosis (Miller *et al.*, 2012). Most patients with CIS will further progress to definite multiple sclerosis (Polman *et al.*, 2011). The underlying pathology of multiple sclerosis is characterized by inflammation, demyelination, axonal injury, and axonal loss leading to a disruption of long- and short-range connections (Zipp *et al.*, 2013). However, the brain is a complex network of structurally and functionally interconnected regions; thus, it is essential to study its topology to better understand pathology (Bullmore and Sporns, 2009). Diffusion tensor imaging (DTI) can map the structural connectivity between grey matter regions using white matter tractography, while functional connectivity examines synchronization in activity between different grey matter regions. Abnormalities in both modalities have previously been depicted in patients with both CIS and multiple sclerosis (Fleischer *et al.*, 2017*a, b*). However, the lack of multimodal studies using structural and functional imaging in early multiple sclerosis makes it challenging to understand the pathophysiological processes occurring at this stage of the disease. A combination of these modalities may help bridge the gap between pathophysiological changes and clinical symptoms. Structural and functional connectivity networks provide a different perspective of brain functioning. However, there is still a poor understanding of how each connectivity evolution relates to the other. Hence, simultaneously assessing structural and functional connectivity may provide complementary views of the brain and enhance our understanding of the disease evolution. Most network studies in patients with multiple sclerosis focus only on a single modality to explore the connectivity, and most have a cross-sectional design that may be insufficient to describe the pathological changes due to the disease. To that end, studies must combine structural and functional connectivity networks in a longitudinal setting to better understand pathological mechanisms in the brain. Functional connectivity has been shown to be shaped and constrained by the underlying anatomy (Honey *et al.*, 2009) and should provide information close to that obtained from structural connectivity. On the other hand, recent studies exploring neurological disorders other than multiple sclerosis have showed that the structural-functional coupling, which represents the association between functional and structural connectivity, allows the detection of more subtle brain alterations than any single imaging modality (Zhang *et al.*, 2011, 2017; Dai *et al.*, 2018). Whether the structural-functional connectivity coupling could also be altered early in the course of multiple sclerosis is currently unknown.

The brain presents a modular structure with networks of densely interconnected regions, which are more sparsely connected with regions in other networks (Newman and Girvan, 2004; Newman, 2006). Recent studies have observed modular-specific alterations in patients with CIS and multiple sclerosis in both structural and functional networks (Gamboa *et al.*, 2014; Kocevar *et al.*, 2016; Muthuraman *et al.*, 2016; Fleischer *et al.*, 2017*a, b*; Liu *et al.*, 2018), suggesting that modular-related properties may be more sensitive than whole-brain and nodal properties in reflecting brain abnormalities. Previously, we reported functional reorganization, especially 1 year after CIS, by depicting a combination of underconnected and overconnected brain regions using the hub disruption index (Koubiyr *et al.*, 2018). This allowed us to demonstrate global brain functional reorganization at this stage of the disease. However, the current study moves beyond the previous one, and intends to investigate both structural and functional connectivity evolution during the first year after CIS, especially at the modular level, and more importantly how these two modalities relate to each other.

In this study, we combined functional and structural connectivity to investigate the longitudinal evolution of both global and modular-specific topology changes in the brain in the first year following CIS. We also hypothesized that because of the nature of multiple sclerosis, the disruption of connections may lead to structural-functional connectivity decoupling, which we investigated at both the modular and whole-brain levels.

Materials and methods

Standard protocol, approvals, registration and patient consent

Each patient provided written informed consent. Patients were included in the prospective study without intervention, analysing early brain damage in patients with CIS (SCICOG, ClinicalTrials.gov Identifier: NCT01865357). This study was approved by the local ethics committee.

Participants

The population used in this study has been described in a previous study (Koubiyr *et al.*, 2018). Briefly, we prospectively recruited 52 consecutive patients with CIS <6 months after an initial neurological episode of the type seen in multiple sclerosis. They presented with at least two clinically silent cerebral lesions on fluid-attenuated inversion recovery (FLAIR) images that were characteristic of multiple sclerosis. These patients underwent MRI scans at baseline, and only 41 patients with CIS were rescanned after 1 year of evolution, as 11 patients were lost to follow-up. The exclusion criteria included: age <18 years, inability to undergo MRI, history of other neurological or psychiatric disorders, multiple sclerosis relapse within 2 months prior to screening, corticosteroid pulse therapy within 2 months prior to screening, and severe depression (Beck Depression Inventory >27). The patients underwent neurological examination by expert neurologists and were scored on the Expanded Disability Status Scale (EDSS) (Kurtzke, 1983) and the Multiple Sclerosis Functional Composite (MSFC) measure (Ontaneda *et al.*, 2012).

Twenty healthy control subjects matched for age, sex and educational level were also included in the study and underwent the same MRI protocol. Nineteen of these were rescanned 1 year after the first assessment.

To study the longitudinal evolution of structural and functional brain network topology, only participants with longitudinal follow-up were considered for the current analyses. All participants were also evaluated using a comprehensive neuropsychological battery (Supplementary Table 1). Detailed neuropsychological results can be found in a previous report (Koubiyr *et al.*, 2018).

Information on the type of CIS can be found in Table 1. Additionally, to assess patients' lesion topography, we computed a lesion frequency map for our CIS patients (Supplementary Fig. 1). As it can be seen from this frequency map and from Table 1, our patients' lesion load is rather small, and the low lesion frequency indicates that lesion topography varies from one patient to another. In addition to that, as the number of patients per type of symptoms is small, it is not possible to interpret abnormalities in specific networks according to type of onsets.

MRI acquisition

MRI acquisition was performed on a 3 T MRI system (Achieva TX system, Philips Healthcare; Sigma, GE Healthcare, Discovery MR 750w). The acquisition protocol was harmonized between the magnets and consisted of a 3D T_1-weighted sequence using magnetization prepared rapid gradient echo imaging (MP-RAGE, repetition time = 8.2 ms, echo time = 3.5 ms, inversion time = 982 ms, $\alpha = 7^\circ$, field of view = 256 mm, voxel size = 1 mm^3, 180 slices), a 2D FLAIR sequence (repetition time = 11 000 ms, echo time = 140 ms, inversion time = 2800 ms, field of view = 230 mm, 45 axial slices, 3-mm slice thickness), a diffusion tensor echo-planar imaging pulse sequence (repetition time = 11 676 ms, echo time = 60 ms, field of view = 230 mm, an isotropic resolution of $1.6 \times 1.6 \times 1.6$ mm^3 and b = 1000 s/mm^2) in 21 non-colinear directions, and one b = 0 s/mm^2. Resting-state functional MRI was obtained with an echo-planar imaging sequence (250 volumes, 40 axial slices, repetition time = 2200 ms, echo time = 30 ms, 3×3-mm in-plane resolution, and 3-mm slice thickness).

Structural preprocessing and anatomical parcellation

Lesions were segmented on FLAIR data using the Lesion Segmentation Tool version 2.0.15 (http://www.applied-statistics.de/lst.html) in Statistical Parametric Mapping (SPM12; www.fil.ion.ucl.ac.uk/spm). They were then manually corrected by two blinded experts. Using these maps, a lesion-filling algorithm (Prados *et al.*, 2016) was applied to the T_1-weighted images to avoid the lesions affecting brain tissue segmentation. Whole-brain, total white matter, grey matter and CSF volumes were calculated using the volBrain system (http://volbrain.upv.es) (Manjón and Coupé, 2016).

Structural data were preprocessed with the FreeSurfer (v5.3) image analysis suite, which was documented and is freely available online (http://surfer.nmr.mgh.harvard.edu) (Dale *et al.*, 1999). The brain was separated into regions of interest using a custom-made atlas. The cortical atlas was

Table 1 Demographic, clinical and conventional MRI characteristics

Clinical features	Baseline		Year 1	
	HC (*n* = 19)	CIS (*n* = 41)	HC (*n* = 19)	CIS (*n* = 41)
Mean age, years (SD)[a]	37.8 (8.6)	38.3 (11.2)	-	-
Sex ratio, F/M[b]	14/5	32/9	-	-
Education level, high/low[b,c]	10/9	26/15	-	-
Symptoms at clinical onset:				
Brain	-	4 (10%)	-	-
Optic neuritis	-	7 (17%)	-	-
Brainstem/cerebellar	-	11 (27%)	-	-
Spinal cord	-	19 (46%)	-	-
Mean disease duration (SD) in months	-	4.12 (1.85)		
Median EDSS score [range][d]	-	1.0 [0–3]	-	1.0 [0–5]
MSFC z-score (SD)[d]	-	0.32 (0.41)	-	0.31 (0.60)
Median T_2 lesion volume, ml[d]	-	0.98 [0.02–63.12]	-	1.32 [0.07–67.74]
Normalized brain fraction, %[e,f]	86.41 ± 2.95	84.59 ± 4.08	86.39 ± 3.02	83.75 ± 4.11*
Normalized white matter fraction, %[g,e,f]	36.59 ± 2.42	35.52 ± 3.13	37.28 ± 3.14	34.51 ± 3.27**
Normalized grey matter fraction, %[e,f]	49.82 ± 2.58	49.07 ± 2.85	49.11 ± 2.31	49.25 ± 2.86
Normalized CSF fraction, %[e,f]	13.59 ± 2.95	15.41 ± 4.08	13.61 ± 3.02	16.25 ± 4.11*

[a]Mann–Whitney U-test.
[b]χ^2 test.
[c]Education level was considered as high or low according to a French baccalaureate.
[d]Wilcoxon test to compare patients with CIS at baseline and 1 year.
[e]GLM comparing patients with CIS to healthy control subjects with age, sex, level of education, and scanner as covariates.
[f]Percentage: (structure's volume/TIV) × 100.
Differences between patients with CIS and healthy controls: *$P < 0.05$; **$P < 0.01$.
EDSS = Expanded Disability Status Scale; HC = healthy controls; SD = standard deviation; TIV = total intracranial volume.

derived from the Destrieux cortical atlas (Destrieux *et al.*, 2010), which was based on a parcellation scheme that first divided the neocortex into gyral and sulcal regions, with the limit between both being given by the curvature value of the surface. Other grey matter structures (thalamus, pallidus, accumbens, putamen, caudate and amygdala, hippocampus), the cerebellar cortex, and the ventral diencephalon, as segmented by FreeSurfer, were also included as regions of interest. Finally, our custom-made atlas included 83 regions per hemisphere.

T_1-weighted images were registered to diffusion images (B0 image as a reference) by a rigid registration followed by a non-rigid registration of the T_1-weighted image to the subject's B0 space using ANTs software (Avants *et al.*, 2011). Registration between the functional MRI and the T_1-weighted sequences was performed using boundary-based registration.

The complete atlas was then co-registered to each participant's functional MRI and diffusion scans, and all registrations were visually checked.

DTI preprocessing

Diffusion data were preprocessed using the Oxford Centre for Functional MRI of the Brain Software Library (version 5.0.9; fsl.fmrib.ox.ac.uk/fsl). Eddy current distortions and motion artefacts were corrected, and brain tissue was extracted. Subsequently, MRtrix3 software (Tournier *et al.*, 2012) was used for diffusion-weighted tractography. First, a single-shell response function was estimated (Tournier *et al.*, 2013) to calculate the fibre orientation distributions using the constrained spherical-deconvolution algorithm (Tournier *et al.*, 2007). Five tissue-type segmented T_1 image and anatomically constrained tractography (Tournier *et al.*, 2012) were used to generate 10 million whole-brain tracts. These tracts were cropped at the grey–white matter interface. Finally, these streamlines were filtered to 2 million using the spherical-deconvolution informed filtering of tractograms (Smith *et al.*, 2013) to reduce reconstruction bias and improve biological plausibility.

Resting-state functional MRI preprocessing

Using SPM12, we followed the same functional MRI preprocessing that was used in a previous study (Koubiyr *et al.*, 2018). Briefly, the constant offset and linear trend over each run were removed, a low-pass temporal filter with a 0.08-Hz cut-off was applied, and the data were slice time-corrected. Sources of spurious variance, as well as their temporal derivatives, were removed through linear regression, including the following: (i) six parameters obtained via correction of rigid body head motion; (ii) the signal averaged over the whole brain; (iii) the signal averaged over the ventricles; and (iv) the signal averaged over the deep cerebral white matter. This regression procedure contributed to the minimization of signal contributions of non-neuronal origin, including respiration-induced signal fluctuations (Van Dijk *et al.*, 2010). The first four volumes of the functional run were discarded to achieve steady-state magnetization.

Brain network construction

Structural connectome construction

Streamlines previously obtained from tractography were mapped into the 166 atlas nodes to produce a 166×166 weighted structural connectivity matrix. Each element of the structural connectivity matrix represented the streamline counts normalized by the total number of tracts for each participant, to correct for seed region size.

Functional connectome construction

To construct the functional connectivity matrix, for each participant, the average BOLD (blood oxygen level-dependent imaging) time courses were extracted from each of the 166 regions defined by our final atlas. Pearsons linear correlation coefficients were then computed between the signals from all pairs of regions. A Fisher's Z-transformation was further applied to the correlation matrices to improve the normality of the correlation coefficient, leading to a 166×166-weighted functional connectivity matrix. Given the controversial nature of the physiological meaning of negative correlations (Chang and Glover, 2009; Anderson *et al.*, 2011), the elements of significantly negative correlations were set to zero.

Network characteristics

We conducted graph theoretical network analysis to investigate the overall topological properties of whole-brain networks in patients with CIS and healthy control subjects. These analyses were carried out on the functional and structural connectivity networks of each participant using the Brain Connectivity Toolbox (http://www.brain-connectivity-toolbox.net) (Rubinov and Sporns, 2010). We calculated segregation properties (clustering coefficient), centrality properties (degree, betweenness centrality), and integration properties (global efficiency). These measures were detailed in Rubinov and Sporns (2010). Briefly, the clustering coefficient represented the fraction of the node's neighbours that were also neighbours of each other. The degree of a node was the sum of all connections between this node and other nodes. Betweenness centrality was defined as the fraction of all the shortest paths in the network that pass through a given node. Global efficiency was the average inverse shortest path length and could estimate the efficiency with which brain regions communicated.

To verify the robustness of our brain parcellation to the network metrics, we generated new parcellation schemes with approximately half the number of original regions by combining pairs of adjacent regions as in Fagerholm *et al.* (2015). Then, structural and functional connectivity matrices were computed again from this new parcellation and network measures were calculated. As a region may have more than one adjacent neighbour in the original parcellation, we randomly selected the neighbouring region to be combined. We repeated this process 30 times with different randomly selected adjacent regions to ensure stability.

Modularity

To identify brain functional modules (i.e. a set of densely intraconnected networks), we conducted a modularity analysis on the functional connectivity network. Given that the module

membership varied between participants, we performed the modularity analysis at the group level by averaging functional connectivity matrices of all participants at baseline. Modular analysis aimed to find a specific module partition that yielded a maximum modularity Q^w. Functional modules were detected using the Louvain modularity algorithm (Blondel *et al.*, 2008) combined with a fine-tuning algorithm (Sun *et al.*, 2009). Furthermore, to improve the reliability of the modular structure, this algorithm was repeated 250 times. Finally, we derived a consensus partition using the method described by Lancichinetti and Fortunato (2012). The final consensus partition had a modularity of $Q^w = 0.41$ and contained five networks, including the frontoparietal network (FPN), the salience network (SN), the default mode network (DMN), the visual network (VN), and the somatomotor network (SMN; Fig. 1). These networks were visually inspected and corresponded well with resting-state networks reported previously (He *et al.*, 2009; Power *et al.*, 2011; Yeo *et al.*, 2011).

Modular characteristics

To characterize the modular-related topology at the nodal level, we calculated the participation coefficient (PC) that measured the inter-module connectivity of each node. For a node i, PC was calculated as:

$$PC_i = 1 - \sum_{s=1}^{N_M} \left(\frac{k_{is}}{k_i}\right)^2 \quad (1)$$

where N_M is the total number of modules, k_{is} is the number of links of node i to nodes in module s, and k_i is the total degree of node i.

We also computed the within-module degree z-score (WD) that measured the intra-module connectivity of a node. For a node i, WD was calculated as:

$$WD_i = \frac{k_i - k_{s_i}}{\sigma_{k_{s_i}}} \quad (2)$$

where k_i is the number of links of the node i, k_{s_i} is the average of the degree over all nodes in s_i, and $\sigma_{k_{s_i}}$ is the standard deviation of the degree in s_i.

Participation coefficient (PC) ranged from 0 to 1, where PC was close to 1 if node i had a homogeneous connection distribution with all the modules, and 0 if node i was exclusively linked to other nodes in its own module. WD, on the other hand, was large for a node i that had many intra-module connections relative to other nodes in the same module. These modular parameters were computed for both structural and functional networks.

Structural–functional connectivity coupling

We assessed structural-functional connectivity coupling as the correlation coefficient between strengths of the structural and functional networks. For each participant, this correlation was constrained by edges of non-zero structural connectivity. Specifically, non-zero structural connectivity edges were extracted to form a vector of structural connectivity values, which was further rescaled into a Gaussian distribution (Honey *et al.*, 2009). Functional connectivity was then extracted to form a corresponding vector. Finally, structural-functional connectivity coupling was quantified by the Pearson's coefficient of correlation between the two previous vectors. We evaluated structural-functional connectivity coupling both at the whole-brain level and in each module.

Statistical analysis

Statistical analyses were performed using MATLAB 2016a (MathWorks, Natick, MA, USA) and SPSS 23.0 (SPSS, Chicago, IL, USA).

Normality of distribution was assessed by the Shapiro–Wilk test. Categorical variables were investigated with χ^2 tests, while continuous variables were investigated with two-sample t-tests. To examine between-group differences in network properties, a general linear model analysis was performed with age, gender, education level, and scanner as covariates at each time point. For those network metrics showing significant group differences, a region-wise comparison of the corresponding metric was used to search for the major regions driving this modification. Region-wise comparison of global

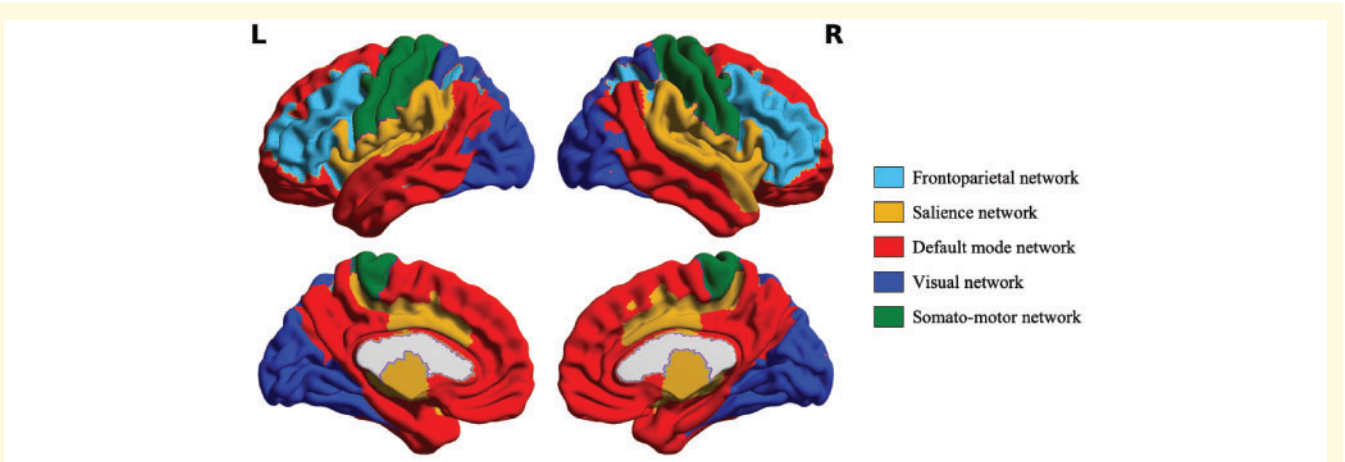

Figure 1 Identified resting-state functional networks.

network metrics and modular metrics was performed using a randomized permutation testing (10 000 permutations) corrected for multiple comparisons (Blair and Karniski, 1993; Groppe *et al.*, 2011) on age-, sex-, education-, and scanner-standardized residuals.

Finally, association between altered connectivity metrics and clinical/neuropsychological scores was analysed using linear regression models where age, sex, and education level were considered as nuisance variables.

Data availability

The data that supported the findings of this study are available from the corresponding author upon reasonable request.

Results

Clinical, neuropsychological and conventional MRI characteristics

The characteristics of both patients with CIS and healthy control subjects are summarized in Table 1. The two groups were matched for age, sex, and level of education at each time point. In patients with CIS, the EDSS and MSFC scores did not change significantly between baseline [median EDSS = 1, range = 0–3; mean MSFC = 0.32, standard deviation (SD) = 0.41] and Year 1 (median EDSS = 1, range = 0–5; mean MSFC = 0.31, SD = 0.60), and T_2 lesion volumes (T_2 LV) did not differ significantly between baseline (median T_2 LV = 0.98 ml, range = 0.02–63.12 ml) and Year 1 (median T_2 LV = 1.32 ml, range = 0.07–67.74 ml).

At baseline, patients with CIS did not differ from healthy control subjects in whole normalized brain, white matter, grey matter, and total CSF volumes. However, after 1 year, patients with CIS developed global brain atrophy with decreased whole-brain and white matter volumes ($P < 0.05$) and increased total CSF volume ($P < 0.05$) compared to healthy control subjects (Table 1).

Regarding cognition, patients with CIS showed a moderate cognitive impairment at baseline with alterations on the Computerized Speed Cognitive Test (CSCT) and the Brief Visual Memory Test-Revised (BVMTR). At 1 year, this cognitive impairment was no longer observed.

Structural connectivity network

At baseline, the clustering coefficient was significantly increased in patients compared to healthy control subjects (Fig. 2A), while the degree, betweenness centrality, and global efficiency were unaffected. At the nodal level, we found that these alterations were in the occipital, parietal, temporal, frontal and central regions and in the right pallidum (Fig. 2B and Supplementary Table 4). At the modular level, the participation coefficient was significantly increased in the posterior part of the cingulate and the inferior parietal lobe and decreased in the left central sulcus (Fig. 2C and Supplementary Table 4), while the within-module degree was significantly increased in the superior occipital, postcentral, and middle frontal gyrus (Fig. 2D and Supplementary Table 4).

At Year 1, there was no difference between patients with CIS and healthy control subjects in the overall network metrics (degree, betweenness centrality, clustering coefficient, and global efficiency). However, at the modular level, alterations were still present. The participation coefficient was significantly decreased in patients with CIS compared to healthy control subjects in the bilateral central sulcus and increased in the inferior parietal gyrus (Fig. 2E and Supplementary Table 4); on the other hand, the within-module degree was decreased in the cerebellum and inferior temporal sulcus and increased in the superior frontal sulcus (Fig. 2F and Supplementary Table 4). Using different parcellation schemes, clustering coefficient at baseline was still the only altered parameter as it was significantly increased in patients compared to controls in each case (Supplementary Table 6).

Functional connectivity network

At baseline, no differences were noted in the overall network metrics between patients with CIS and healthy control subjects. This was the same for modular-related metrics (participation coefficient and within-module degree) (Fig. 3A and B).

After 1 year, betweenness centrality was significantly increased in patients with CIS compared to healthy control subjects (0.023 ± 0.002 versus 0.021 ± 0.001; $P = 0.006$); however, no region survived after the multiple comparison correction for the nodal-level comparison. Regarding the modular-related metrics, the participation coefficient significantly increased in patients with CIS compared to healthy control subjects in the right anterior circular sulcus of the insula (Fig. 3C and Supplementary Table 5), while the within-module degree was increased in the right hippocampus and left post-ventral cingulate gyrus, and it was decreased in the bilateral frontomarginal gyrus and sulcus and left temporal pole (Fig. 3D and Supplementary Table 5). Using different parcellation schemes, betweenness centrality at 1-year was again the only altered parameter as it was significantly increased in patients compared to controls in each case (Supplementary Table 7).

Structural-functional connectivity coupling

Both the patients with CIS and healthy control subjects groups showed significant correlations between regional structural and functional connectivity (all $P < 10^{-95}$, correlation coefficient ranging from 0.15 to 0.32). These correlations were still present when looking at the modular level (all $P < 10^{-4}$, ranging from 0.23 to 0.7).

At baseline, structural-functional connectivity coupling was preserved in patients compared to healthy control subjects at both the whole-brain and the modular levels. After

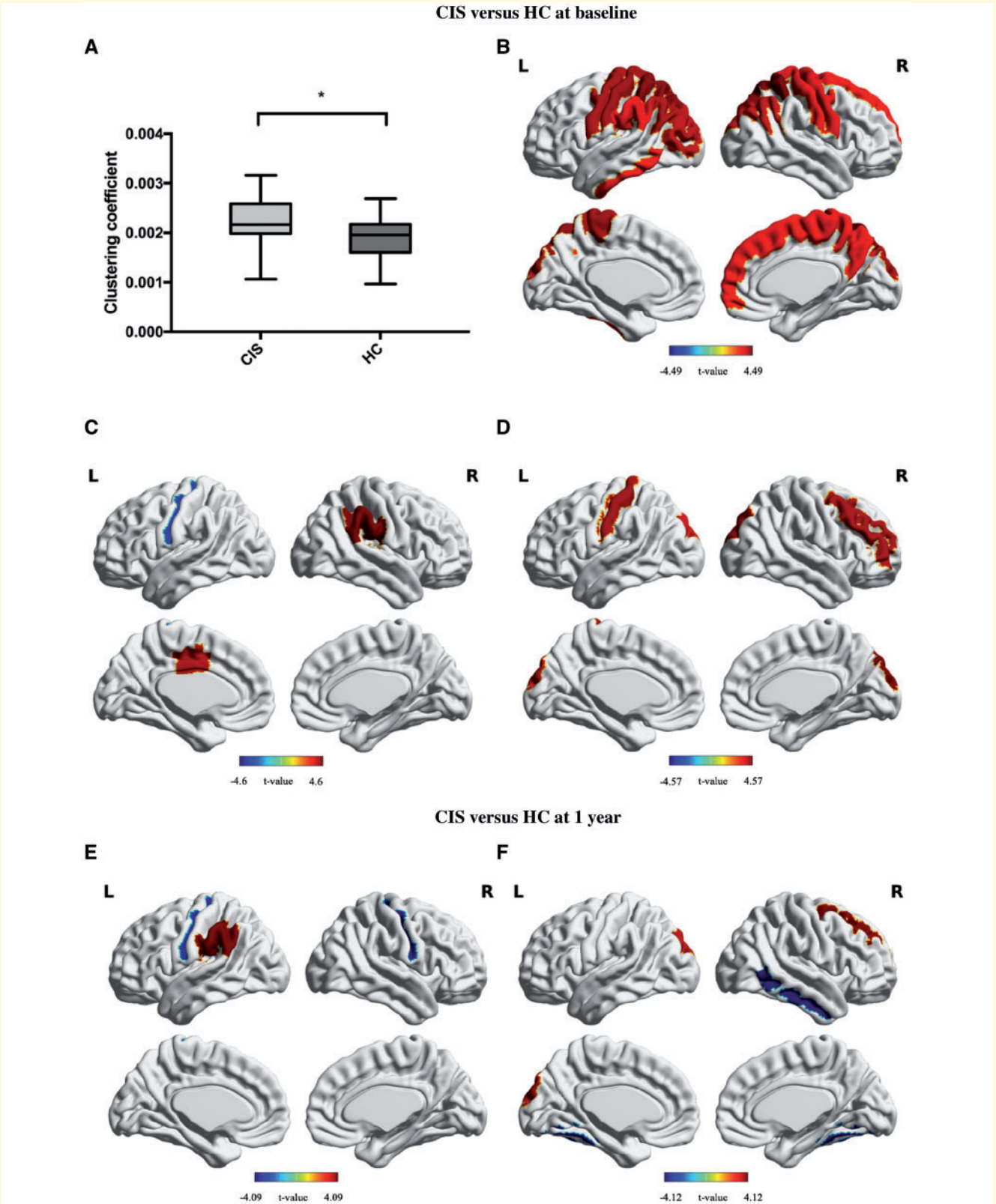

Figure 2 Structural connectivity alterations. (**A**) Overall clustering coefficient comparison. (**B**) Region-wise clustering coefficient comparison. (**C**) Participation coefficient comparison between patients with CIS and healthy control subjects. (**D**) Within-degree module z-score (WD) comparison between patients with CIS and healthy control subjects. (**E**) Participation coefficient comparison between patients with CIS and healthy control subjects, and (**F**) WD comparison between patients with CIS and healthy control subjects. HC = healthy control subjects.

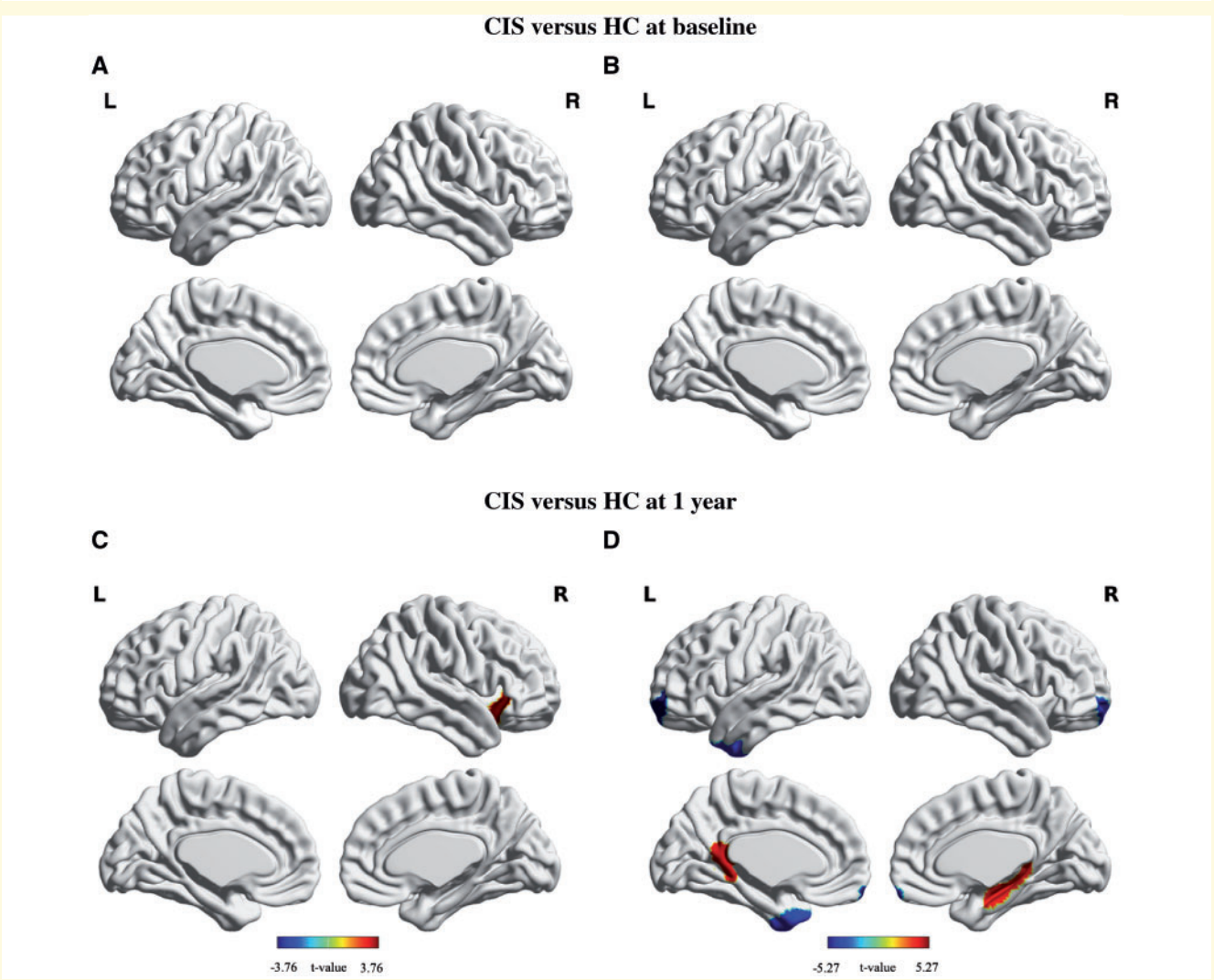

Figure 3 Functional connectivity alterations. (**A**) Participation coefficient comparison between patients with CIS and healthy control subjects at baseline. (**B**) Within-degree module z-score (WD) comparison between patients with CIS and healthy control subjects at baseline. (**C**) Participation coefficient comparison between patients with CIS and healthy control subjects, and (**D**) WD comparison between patients with CIS and healthy control subjects. HC = healthy control subjects.

1 year of evolution, whole-brain coupling was still preserved; however, structural-functional connectivity decoupling was observed in three networks (salience network, visual network and somatomotor network) (Fig. 4).

Clinical and neuropsychological correlates

No association was found between structural-functional connectivity coupling and clinical/neuropsychological variables either at baseline or after 1 year of follow-up.

MSFC at baseline was associated with educational level ($\beta = -0.29$; $P = 0.049$) and DTI clustering coefficient at baseline ($\beta = -0.36$; $P = 0.017$) for a significant model ($P = 0.005$) explaining $R^2_{adj} = 25\%$ of the variance. Conversely, CSCT at baseline was associated with age ($\beta = -0.44$; $P = 0.003$) and DTI clustering coefficient at baseline ($\beta = -0.28$; $P = 0.049$) for a significant model ($P = 0.002$) explaining $R^2_{adj} = 29\%$ of the variance. After 1 year, no clinical/neuropsychological variable was associated with altered network metrics at follow-up.

Discussion

In the present study, we investigated the longitudinal reorganization of both structural and functional brain networks in the first year following CIS. We showed that overall network alterations were already present after the first clinical event, structural damage as the clustering coefficient was increased in patients, and modular-related

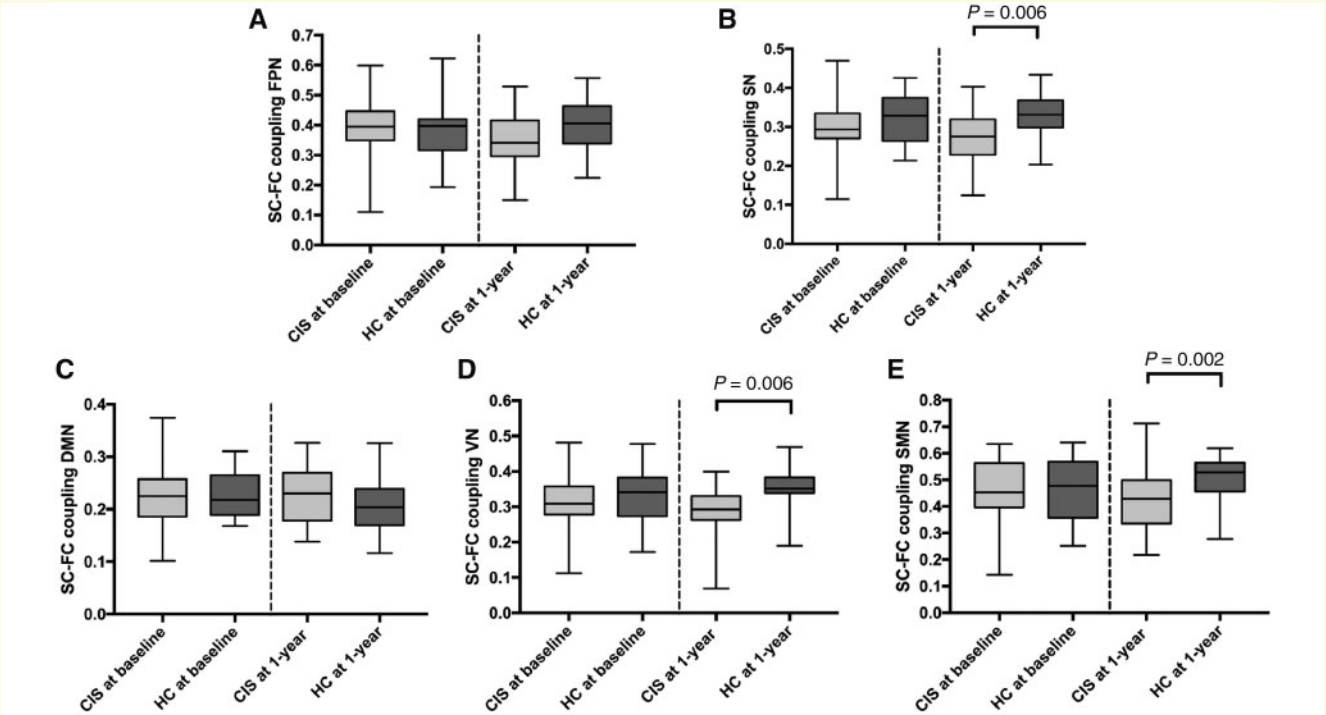

Figure 4 Structural-functional decoupling at the network level at baseline and 1 year. DMN = default mode network; FPN = frontoparietal network; HC = healthy control subjects; SC-FC = structural-functional connectivity; SMN = somatomotor network; SN = salience network; VN = visual network.

structural connectivity was altered. In particular, increased clustering coefficient was associated with clinical and cognitive deficit at baseline (MSFC and CSCT). After 1 year of evolution, both structural and functional reorganizations were observed with altered modular-related connectivity, and there was an increase of betweenness centrality in the functional network. At this stage, structural-functional connectivity decoupling in three modules was also noticed, together with the previous abnormalities.

Modularity has been considered as one of the main properties of brain network organization, leading to the functional specialization and segregation of the brain (Bullmore and Sporns, 2009). Specifically, we identified five densely intraconnected networks, which corresponded to the well-known functional modules frontoparietal, salience, default mode, visual, and motor/sensorimotor networks (He *et al.*, 2009; Power *et al.*, 2011; Yeo *et al.*, 2011).

At the clinical onset, structural damage was already present in patients with CIS, as we observed an increased clustering coefficient. Clustering coefficient, which has recently been shown to be increased in patients with early relapsing-remitting multiple sclerosis (Fleischer *et al.*, 2017*a, b*) indicated the strengthening of short distance connections to preserve local information flow. This was also shown by the increased within-module degree inside the fronto-parietal network, visual network, and somatomotor network, which could be considered favourable for behaviours that required specialized processing (Park and Friston, 2013). In addition, the participation coefficient was increased in regions of the salience network and decreased in some other region of the somatomotor network. Alterations in these modular parameters in one direction or the other could inform on the ability of a region to recruit alternative routes. Ultimately, it is suggested that the brain is seeking the best trade-off with lower metabolic connection costs at the expense of losing integrative capacity by rerouting and reweighting its connections (Bullmore and Sporns, 2012). This type of reorganization has been observed in other neurological disorders such as Alzheimer's disease (Lo *et al.*, 2010) or Parkinson's disease (Hall *et al.*, 2018).

Importantly, the overall functional network was still preserved at this stage of the disease, although structural abnormalities were observed, which was in line with the recent results from Liu *et al.* (2018).

After 1 year of evolution, in addition to alterations within the structural network, functional reorganization appeared with an increased overall betweenness centrality and increased participation coefficient in the anterior insula sulcus, along with modifications of within-module degree within the DMN. These results supported the hypothesis that structural damage could precede functional changes in multiple sclerosis and needed to achieve a certain threshold to cause these functional modifications (Schoonheim *et al.*, 2015).

Structurally-connected grey matter regions showed stronger functional connectivity than structurally-unconnected

regions, which led us to believe that structural connectivity could predict the functional connections (Hagmann *et al.*, 2008; Honey *et al.*, 2009). However, functional connectivity was not constant, and it was continuously reconfigured around the underlying anatomy through plasticity (Hagmann *et al.*, 2010). Therefore, the structural-functional connectivity coupling could be informative and was found to be decreased in other neurological diseases, such as epilepsy (Zhang *et al.*, 2011), stroke (Zhang *et al.*, 2017) or Alzheimer's disease (Dai *et al.*, 2018). Here, we investigated for the first time the structural-functional connectivity coupling in the early stages of multiple sclerosis. We observed a preserved coupling at the whole-brain level during follow-up; however, when looking at the modular level, structural-functional connectivity decoupling was noticed in the salience network, visual network, and somatomotor network. These findings, along with the increased functional connectivity at 1 year, suggest that functional reorganization involves new functional connections, occurring across structurally-unconnected regions.

Only a moderate cognitive impairment was noted at baseline, as the CSCT and BVMTR scores were the only scores to be significantly decreased in patients with CIS compared to healthy control subjects. Multiple sclerosis attacks have been known to impact cognitive performances; this is known as the post-relapse effect. However, this effect is no longer observed between 1 to 3 months after the attack (Benedict *et al.*, 2014; Giedraitiene *et al.*, 2018). As our patients were included 2 to 6 months after their first episode, we postulate it is unlikely these early cognitive deficits depend on this effect. Additionally, worse CSCT performance and a lower MSFC score were associated with early structural damage (altered structural clustering coefficient). However, there was no more cognitive impairment at follow-up, and the global clinical state also did not worsen (MSFC and EDSS scores were not different from baseline). We have previously shown that functional reorganization occurring 1 year after CIS was associated with better cognitive performance (Koubiyr *et al.*, 2018). Thus, it could be suggested that functional reorganization at this stage was able to compensate for the first deficits through indirect structural connections, and this compensation could fail once the structural damage was too widespread and functional rerouting was less efficient. One other explanation for normal cognitive performance at 1 year could come from the preserved structural-functional connectivity coupling in the DMN because connectivity alterations in the default mode network were strongly associated with cognitive deficits at different stages of multiple sclerosis in previous studies (Louapre *et al.*, 2014; Eijlers *et al.*, 2017). However, a longer follow-up will be needed to confirm these statements.

The current study is not without limitations. First, structural-functional connectivity coupling is only computed for anatomically connected regions; however, functional connectivity can also result from indirect structural paths (Honey *et al.*, 2009). More sophisticated computational models are needed to consider these pathways and their effect on the functional connectome. Additionally, as structural connectivity investigates white matter bundles and functional connectivity investigates synchronization between two grey matter regions, there is no anatomical overlay between these two modalities, making it impossible to use a voxel-wise approach, which explains our choice (and previous studies) to use a Pearson correlation coefficient between vectors representing each connectivity. Second, our DTI data cover only 21 directions in the whole sphere as a trade-off to the good resolution obtained. This could have an effect on our tractography estimation. However, this effect would be present in CIS patients and in healthy control subjects as well, which could limit its influence. Also, our data were acquired on two different scanners. To the best of our ability, we harmonized the protocols between the two magnets. For DTI, we have applied exactly the same directions to cover the whole sphere and obtained the same resolution. This was also the case for functional MRI as we used the same acquisition parameters as well as the same number of runs. An *et al.* (2017) tested the intervender reliability of the resting-state functional MRI and showed that this modality could be highly reliable among different scanners. To correct for this parameter even more, we included the scanner variable as a covariable in all of our analyses. Regarding the five modules we obtained in our analyses, they were detected using the Louvain algorithm, which automatically detects regions synchronously connected to each other during the whole scan time and assigns them to the same network. Additionally, we repeated this algorithm 250 times and derived the consensus modules to improve our reliability. We detailed this procedure in the 'Materials and methods' section. As a result, we do not control the number of modules, as well as the regions belonging to each one of them. We acknowledge the potential presence of more networks; however, we do not have the spatial or temporal resolution, nor a very high number of subjects to separate them from the obtained modules. Once our modules were obtained, we compared them with the literature and found a good correspondence (He *et al.*, 2009; Power *et al.*, 2011; Yeo *et al.*, 2011). Other studies investigating different neurological disorders have found a similar number of modules in their analysis (Rudie *et al.*, 2013; Shin *et al.*, 2014; Sun *et al.*, 2017; Dai *et al.*, 2018). Finally, we only estimate functional connectivity as the mean of the entire recording. However, functional connectome has been shown to possess dynamic properties that may depend on the underlying anatomy (Shen *et al.*, 2015). Even though this is not the scope of our study, this question remains important for future understanding of the pathology.

In conclusion, the current study demonstrated structural damage preceding functional reorganization and possible compensation at both the whole-brain and network levels during the first year following CIS. For the first time, we showed structural-functional connectivity decoupling in

some brain networks in multiple sclerosis, suggesting that functional reorganization occurs along indirect anatomical pathways.

Acknowledgements

The authors thank the neurologists of the AQUISEP network for their involvement in recruiting patients. The authors thank Dr JC Ouallet, Dr A Moroso, and Dr P Louiset for referring patients to the study.

Funding

The authors disclose receipt of the following financial support for the research, authorship, and/or publication of this article: This study was supported by the Translational Research and Advanced Imaging Laboratory (TRAIL), laboratory of excellence (ANR- 10-LABX-57). The SCI-COG study was also supported by a grant from TEVA and ARSEP (Fondation ARSEP pour la recherche sur la sclérose en plaques). This work has been performed with the help of the French Observatoire of Multiple Sclerosis (OFSEP), which is supported by a grant provided by the French State and handled by the "Agence Nationale de la Recherche", within the framework of the "Investments for the Future" program, under the reference no. ANR-10-COHO-002.

Competing interests

B.B. reports grants from the French Ministry of Health during the conduct of the study; personal fees and non-financial support from Biogen-idec, grants from Merck-serono, personal fees and non-financial support from Novartis, personal fees and non-financial support from Genzyme, grants, personal fees and non-financial support from TEVA, grants and non-financial support from Bayer, outside the submitted work. A.R. reports grants from TEVA, during the conduct of the study; personal fees and non-financial support from Novartis, personal fees and non-financial support from Biogen, grants, personal fees and non-financial support from TEVA, grants and non-financial support from Roche, grants and non-financial support from Merck, grants and non-financial support from Genzyme, non-financial support from Medday, grants from Bayer, outside the submitted work.

Supplementary material

Supplementary material is available at *Brain* online.

References

An HS, Moon WJ, Ryu JK, Park JY, Yun WS, Choi JW, et al. Intervender and test-retest reliabilities of resting-state functional magnetic resonance imaging: Implications for multi-center imaging studies. Magn Reson Imaging 2017; 44: 125–30.

Anderson JS, Druzgal TJ, Lopez-Larson M, Jeong EK, Desai K, Yurgelun-Todd D. Network anticorrelations, global regression, and phase-shifted soft tissue correction. Hum Brain Mapp 2011; 32: 919–34.

Avants BB, Tustison NJ, Song G, Cook PA, Klein A, Gee JC. A reproducible evaluation of ANTs similarity metric performance in brain image registration. Neuroimage 2011; 54: 2033–44.

Benedict RHB, Morrow S, Rodgers J, Hojnacki D, Bucello MA, Zivadinov R, et al. Characterizing cognitive function during relapse in multiple sclerosis. Mult Scler J 2014; 20: 1745–52.

Blair RC, Karniski W. An alternative method for significance testing of waveform difference potentials. Psychophysiology 1993; 30: 518–24.

Blondel VD, Guillaume JL, Lambiotte R, Lefebvre E. Fast unfolding of communities in large networks. J Stat Mech Theor 2008; 10: P10008.

Bullmore E, Sporns O. Complex brain networks: graph theoretical analysis of structural and functional systems. Nat Rev Neurosci 2009; 10: 312.

Bullmore E, Sporns O. The economy of brain network organization. Nat Rev Neurosci 2012; 13: 336–49.

Chang C, Glover GH. Effects of model-based physiological noise correction on default mode network anti-correlations and correlations. Neuroimage 2009; 47: 1448–59.

Dai Z, Lin Q, Li T, Wang X, Yuan H, Yu X, et al. Disrupted structural and functional brain networks in Alzheimer's disease. Neurobiol Aging 2018; 75: 71–82.

Dale AM, Fischl B, Sereno MI. Cortical surface-based analysis: I. Segmentation and surface reconstruction. Neuroimage 1999; 9: 179–94.

Destrieux C, Fischl B, Dale A, Halgren E. Automatic parcellation of human cortical gyri and sulci using standard anatomical nomenclature supplemental. Neuroimage 2010; 53: 1–15.

Eijlers AJC, Meijer KA, Wassenaar TM, Steenwijk MD, Uitdehaag BMJ, Barkhof F, et al. Increased default-mode network centrality in cognitively impaired multiple sclerosis patients. Neurology 2017; 88: 952–60.

Fagerholm ED, Hellyer PJ, Scott G, Leech R, Sharp DJ. Disconnection of network hubs and cognitive impairment after traumatic brain injury. Brain 2015; 138: 1696–709.

Fleischer V, Gröger A, Koirala N, Droby A, Muthuraman M, Kolber P, et al. Increased structural white and grey matter network connectivity compensates for functional decline in early multiple sclerosis. Mult Scler J 2017a; 23: 432–41.

Fleischer V, Radetz A, Ciolac D, Muthuraman M, Gonzalez-Escamilla G, Zipp F, et al. Graph theoretical framework of brain networks in multiple sclerosis: a review of concepts. Neuroscience 2017b; 403: 35–53.

Gamboa OL, Tagliazucchi E, Von Wegner F, Jurcoane A, Wahl M, Laufs H, et al. Working memory performance of early MS patients correlates inversely with modularity increases in resting state functional connectivity networks. Neuroimage 2014; 94: 385–95.

Giedraitiene N, Kaubrys G, Kizlaitiene R. Cognition during and after multiple sclerosis relapse as assessed with the brief international cognitive assessment for multiple sclerosis. Sci Rep 2018; 8: 8169.

Groppe DM, Urbach TP, Kutas M. Mass univariate analysis of event-related brain potentials/fields I: a critical tutorial review. Psychophysiology 2011; 48: 1711–25.

Hagmann P, Cammoun L, Gigandet X, Meuli R, Honey CJ, Van Wedeen J, et al. Mapping the structural core of human cerebral cortex. PLoS Biol. 2008; 6: 1479–93.

Hagmann P, Sporns O, Madan N, Cammoun L, Pienaar R, Wedeen VJ, et al. White matter maturation reshapes structural connectivity

in the late developing human brain. Proc Natl Acad Sci 2010; 107: 19067–72.
Hall JM, Shine JM, Ehgoetz Martens KA, Gilat M, Broadhouse KM, Szeto JYY, et al. Alterations in white matter network topology contribute to freezing of gait in Parkinson's disease. J Neurol 2018; 265: 1353–64.
He Y, Wang J, Wang L, Chen ZJ, Yan C, Yang H, et al. Uncovering intrinsic modular organization of spontaneous brain activity in humans. PLoS One 2009; 4: 5226.
Honey CJ, Sporns O, Cammoun L, Gigandet X, Thiran JP, Meuli R, et al. Predicting human resting-state functional connectivity from structural connectivity. Proc Natl Acad Sci 2009; 106: 2035–40.
Kocevar G, Stamile C, Hannoun S, Cotton F, Vukusic S, Durand-Dubief F, et al. Graph theory-based brain connectivity for automatic classification of multiple sclerosis clinical courses. Front Neurosci 2016; 10: 478.
Koubiyr I, Deloire M, Besson P, Coupé P, Dulau C, Pelletier J, et al. Longitudinal study of functional brain network reorganization in clinically isolated syndrome. Mult Scler 2018. doi: 10.1177/1352458518813108.
Kurtzke JF. Rating neurologic impairment in multiple sclerosis: an expanded disability status scale (EDSS). Neurology 1983; 33: 1444–52.
Lancichinetti A, Fortunato S. Consensus clustering in complex networks. Sci Rep 2012; 2: 336.
Liu Y, Duan Y, Dong H, Barkhof F, Li K, Shu N. Disrupted module efficiency of structural and functional brain connectomes in clinically isolated syndrome and multiple sclerosis. Front Hum Neurosci 2018; 12: 138.
Lo C-Y, Wang P-N, Chou K-H, Wang J, He Y, Lin C-P. Diffusion tensor tractography reveals abnormal topological organization in structural cortical networks in Alzheimer's disease. J Neurosci 2010; 30: 16876–85.
Louapre C, Perlbarg V, García-Lorenzo D, Urbanski M, Benali H, Assouad R, et al. Brain networks disconnection in early multiple sclerosis cognitive deficits: an anatomofunctional study. Hum Brain Mapp 2014; 35: 4706–17.
Manjón JV, Coupé P. volBrain: an online MRI brain volumetry system. Front Neuroinform 2016; 10: 30.
Miller DH, Chard DT, Ciccarelli O. Clinically isolated syndromes. Lancet Neurol 2012; 11: 157–169.
Muthuraman M, Fleischer V, Kolber P, Luessi F, Zipp F, Groppa S. Structural brain network characteristics can differentiate CIS from early RRMS. Front Neurosci 2016; 10: 14.
Newman MEJ. Modularity and community structure in networks. Proc Natl Acad Sci 2006; 103: 8577–82.
Newman MEJ, Girvan M. Finding and evaluating community structure in networks. Phys Rev E 2004; 69: 026113.
Ontaneda D, Larocca N, Coetzee T, Rudick RA. Revisiting the multiple sclerosis functional composite: proceedings from the National Multiple Sclerosis Society (NMSS) task force on clinical disability measures. Mult Scler J 2012; 18: 1074–80.
Park HJ, Friston K. Structural and functional brain networks: from connections to cognition. Science 2013; 80: 342.
Polman CH, Reingold SC, Banwell B, Clanet M, Cohen JA, Filippi M, et al. Diagnostic criteria for multiple sclerosis: 2010 revisions to the McDonald criteria. Ann Neurol 2011; 69: 292–302.
Power JD, Cohen AL, Nelson SM, Wig GS, Barnes KA, Church JA, et al. Functional network organization of the human brain. Neuron 2011; 72: 665–78.
Prados F, Cardoso MJ, Kanber B, Ciccarelli O, Kapoor R, Gandini Wheeler-Kingshott CAM, et al. A multi-time-point modality-agnostic patch-based method for lesion filling in multiple sclerosis. Neuroimage 2016; 139: 376–84.
Rubinov M, Sporns O. Complex network measures of brain connectivity: uses and interpretations. Neuroimage 2010; 52: 1059–69.
Rudie JD, Brown JA, Beck-Pancer D, Hernandez LM, Dennis EL, Thompson PM, et al. Altered functional and structural brain network organization in autism. NeuroImage Clin 2013; 2: 79–94.
Schoonheim MM, Meijer KA, Geurts JJG. Network collapse and cognitive impairment in multiple sclerosis. Front Neurol 2015; 6: 82.
Shen K, Mišić B, Cipollini BN, Bezgin G, Buschkuehl M, Hutchison RM, et al. Stable long-range interhemispheric coordination is supported by direct anatomical projections. Proc Natl Acad Sci 2015; 112: 6473–78.
Shin DJ, Jung WH, He Y, Wang J, Shim G, Byun MS, et al. The effects of pharmacological treatment on functional brain connectome in obsessive-compulsive disorder. Biol Psychiatry 2014; 75: 606–14.
Smith RE, Tournier JD, Calamante F, Connelly A. SIFT: spherical-deconvolution informed filtering of tractograms. Neuroimage 2013; 67: 298–312.
Sun Y, Dai Z, Li J, Collinson SL, Sim K. Modular-level alterations of structure–function coupling in schizophrenia connectome. Hum Brain Mapp 2017; 38: 2008–25.
Sun Y, Danila B, Josić K, Bassler KE. Improved community structure detection using a modified fine-tuning strategy. Europhys Lett 2009; 86: 28004.
Tournier JD, Calamante F, Connelly A. Robust determination of the fibre orientation distribution in diffusion MRI: non-negativity constrained super-resolved spherical deconvolution. Neuroimage 2007; 35: 1459–72.
Tournier J-D, Calamante F, Connelly A. MRtrix: diffusion tractography in crossing fiber regions. Int J Imaging Syst Technol 2012; 22: 53–66.
Tournier JD, Calamante F, Connelly A. Determination of the appropriate b value and number of gradient directions for high-angular-resolution diffusion-weighted imaging. NMR Biomed 2013; 26: 1775–86.
Van Dijk KRA, Hedden T, Venkataraman A, Evans KC, Lazar SW, Buckner RL. Intrinsic functional connectivity as a tool for human connectomics: theory, properties, and optimization. J Neurophysiol 2010; 103: 297–321.
Yeo BTT, Krienen FM, Sepulcre J, Sabuncu MR, Lashkari D, Hollinshead M, et al. The organization of the human cerebral cortex estimated by intrinsic functional connectivity. J Neurophysiol 2011; 106: 1125–65.
Zhang Z, Liao W, Chen H, Mantini D, Ding JR, Xu Q, et al. Altered functional-structural coupling of large-scale brain networks in idiopathic generalized epilepsy. Brain 2011; 134: 2912–28.
Zhang J, Zhang Y, Wang L, Sang L, Yang J, Yan R, et al. Disrupted structural and functional connectivity networks in ischemic stroke patients. Neuroscience 2017; 364: 212–25.
Zipp F, Gold R, Wiendl H. Identification of inflammatory neuronal injury and prevention of neuronal damage in multiple sclerosis. JAMA Neurol 2013; 70: 1569–74.